Surface & Coatings Technology 335 (2018) 1–12

Contents lists available at ScienceDirect

Surface & Coatings Technology

journal homepage: www.elsevier.com/locate/surfcoat

Influence of feedstock powder and cold spray processing parameters on microstructure and mechanical properties of Ti-6Al-4V cold spray depositions

Venkata Satish Bhattiprolu[a], Kyle W. Johnson[b], Ozan C. Ozdemir[c], Grant A. Crawford[a,*]

[a] Department of Materials and Metallurgical Engineering, South Dakota School of Mines and Technology, Rapid City, SD 57701, USA
[b] VRC Metal Systems, 525 University Loop, Suite 211, Rapid City, SD 57701, USA
[c] Department of Mechanical and Industrial Engineering, Northeastern University, Boston, MA 02115, USA

ARTICLE INFO

Keywords:
Cold spray
Ti-6Al-4V
Feedstock powder
Microstructure characterization
Porosity
Adhesion strength

ABSTRACT

A high pressure cold spray system was used to deposit three Ti-6Al-4V feedstock powders (i.e., hydride de-hydride, plasma atomized, and gas atomized) on Ti-6Al-4V substrates while varying gas temperature and nozzle length. Particle impact temperature and particle velocity were calculated using a 1-D axial model. The microstructure of the feedstock powders and the cold spray depositions were characterized via optical and scanning electron microscopy. The hardness of the as-received powders was determined using nanoindentation. To assess deposition quality, coatings were characterized in terms of porosity, microhardness, and adhesion strength. Results showed that hydride de-hydride powders were characterized by an equiaxed alpha grain structure with intergranular beta phase regions while atomized powders were characterized by martensitic α phase structures. Cold sprayed coatings revealed two distinct microstructures. Regions that experienced low/moderate plastic strain retained the as-received powder microstructure while regions that experienced significant plastic strain were characterized either by a featureless microstructure (atomized coatings) or the presence of fine, elongated beta precipitates (hydride de-hydride coatings). Depositions performed using a long nozzle resulted in the best deposition quality, with porosity as low as 0.3% and adhesion strengths > 69 MPa. While atomized powders resulted in comparatively higher quality coatings for all process conditions, hydride de-hydride coatings of excellent quality (average porosity ≈ 0.6%, adhesion strength > 65 MPa) were achieved under optimal conditions. Thus, hydride de-hydride powders may hold promise as a cost effective alternative to atomized powders for Ti-6Al-4V cold spray depositions.

1. Introduction

Titanium (Ti) and Ti alloys are well known for their high strength-to-weight ratio and excellent corrosion resistance. Consequently, these materials are commonly used in the aerospace industry. In fact, a significant growth in Ti alloy raw material usage in the aerospace industry is projected over the next several years (173 million pounds in 2015 to 212 million pounds by 2020) [1]. This utilization would be even higher if not for the high cost of Ti alloys when compared to competing aerospace alloys such as aluminum and steel. A recent study shows that the production cost for a pound of Ti sheet to be 10–15 times higher than aluminum [2]. Owing to the high cost of manufacturing Ti and Ti alloy aerospace parts, a large market exists for maintenance repair and overhaul (MRO) of aerospace components [5]. One technology that has garnered significant interest in this regard is cold spray processing. The use of cold spray processing in repair and refurbishment of aerospace components is well documented and extensive case studies have been carried out previously [6,7], however, this technology is not yet mature for Ti and Ti alloys.

Cold spray is a solid state deposition process which relies on severe plastic deformation [8,9] of micron scale (< 100 μm) powder particles [10] upon impact with a target substrate, whereby the particles bond to the substrate through a combination of mechanical interlocking and metallurgical bonding [11]. As a solid state deposition process, one of the important advantages of cold spray is that thermally induced phase changes and stress development are limited during deposition. By contrast, high temperature thermal spray processes (e.g. plasma spray, high velocity oxy fuel) often result in the formation of thermal stresses and undesired oxides. The latter can be detrimental to oxygen sensitive materials such as Ti.

* Corresponding author.
E-mail address: grant.crawford@sdsmt.edu (G.A. Crawford).

https://doi.org/10.1016/j.surfcoat.2017.12.014
Received 27 July 2017; Received in revised form 5 December 2017; Accepted 6 December 2017
Available online 06 December 2017

Cold spray technology is now well established for highly deformable face center cubic (FCC) alloys such as aluminum and copper [12–16]. Owing to their higher strength and somewhat limited capacity for plastic strain, Ti and Ti alloys are less amenable to cold spray processing and recent efforts have largely resulted in depositions with poor properties. In this regard, extensive work characterizing the deformation behavior of single particles (single splats) of commercially pure (CP)-Ti [10,17] and Ti-6Al-4V [18,19] have been conducted previously. Goldbaum et al. demonstrated that particles exhibit significant deformation during cold spray processing resulting in non-uniform hardness within the powder particles (i.e. high hardness in the impact region, lower hardness in the jetting region and in upper regions of the splats) [17]. In a separate study, Goldbaum et al. reported high adhesion strengths of up to 250 MPa for Ti-6Al-4V splats deposited using helium gas on Ti-6Al-4V substrates, pre-heated to 400 °C [18]. For this work, adhesion strength was measured using the splat adhesion technique (also known as modified ball bond shear test) [18]. While the measurement may be limited in the ability to predict full coating properties in some systems (considering it does not account for particle-particle interaction and associated porosity development during cold spray deposition), Goldbaum et al. have reported good correlation between splat adhesion strength and coating cohesion strength for titanium coatings sprayed on unheated substrates at low velocities (< 700 m/s) [18]. Blose et al. [4] conducted cold spray deposition of Ti-6Al-4V and reported porosities of roughly 5% and deposition efficiency of ~85%. The porosity reported by Blose et al. was the lowest observed in their study and resulted by increasing the stagnation gas pressure and temperature. It is well established that increasing gas temperature and pressure during cold spray depositions increases particle velocities and can result in improved deposition quality [20–22]. Blose et al. also reported a significant decrease in porosity (roughly 1 to 2%) with powder heating. Recently, porosity of < 1% was reported for cold sprayed Ti-6Al-4V coatings with helium carrier gas, deposited using plasma atomized powders [23]. While the low porosity reported by these authors is encouraging, the tensile strength and ductility of the coating was lower than bulk Ti-6Al-4V, even after applying a post-deposition heat treatment [23]. Clearly the use of a light gas like helium, instead of nitrogen, can effectively improve the deposition quality (especially porosity) [24]. The above studies show the potential for cold spray deposition of Ti-6Al-4V powders with good deposition quality. They also reinforce the importance of an in-depth understanding of the relationships between cold spray processing parameters and deposition quality/properties. Vidaller et al. [19] reported the influence of substrate material for deposition of Ti-6Al-4V splats and suggested the ideal combination to be deposition of Ti-6Al-4V powders on rough Ti/Ti-6Al-4V substrates. Grit blasting prior to cold spray deposition can serve two purposes, i.e. roughening the substrate and removing the inherent oxides on the substrate to improve bonding [25]. Detailed microstructure characterization of Ti-6Al-4V plasma atomized feedstock powder was reported by Birt et al. [26] for their use in cold spray applications. The same group of researchers reported the microstructure evolution of the powders during cold spray deposition and showed the presence of both textured and smooth regions within an individual particle that developed as a consequence of the degree of local plastic strain [27].

Based on the previous reports on cold sprayed Ti-6Al-4V coatings, it is apparent that processing parameters play a significant role in influencing the deposition quality (e.g. porosity). However, studies showing good deposition quality/properties are limited. Thus, there is a critical need for an in-depth understanding of the relationships between processing conditions and deposition quality/properties. Moreover, feedstock powder microstructure is known to significantly influence mechanical properties [28,29]. In this regard, gas atomization (GA), plasma atomization (PA), and hydride de-hydride (HDH) powders are extensively used in the powder metallurgy industry [30–32] and hence are viable options for cold spray. The atomization process involves the formation (i.e. breakup, dispersion, spheroidization) of micron scale liquid droplets from molten metal, followed by rapid cooling and associated solidification, resulting in highly uniform spherical metal powders. Among the various atomization processes, GA and PA are common; however, they differ significantly with respect to the form of the source metal, atomization mechanism, and cooling rates. In plasma atomization, Ti-6Al-4V is introduced as a wire (solid form) [31], whereas in gas atomization it is introduced in a liquid form [33]. As the name suggests, plasma is used for breakup and dispersion of molten metal in plasma atomization and argon gas (at high pressure and velocity) is used in the case of gas atomization. The cooling rates for plasma and gas atomization are 100–1000 °C/s [31] and 1000–10,000 °C/s [33], respectively. Hydride de-hydride (HDH) powder production is generally considered to be a lower cost process [32] and involves hydrogenation of Ti-6Al-4V at 650–700 °C, followed by milling and eventual de-hydrogenation at 350 °C in vacuum to form HDH Ti-6Al-4V powder. Due to the drastic difference in processing temperatures and cooling rates between atomization and HDH processes, the microstructure of the powders resulting from these processes are also different [28,31,34]. As such, the powders are expected to exhibit different deformation characteristics.

In the limited work reported on cold sprayed Ti-6Al-4V coatings, a comprehensive study on the influence of feedstock powder microstructure and cold spray processing conditions (e.g. nozzle length) on cold sprayed Ti-6Al-4V coating microstructure and properties has not been reported. Thus, this work has been conducted as a first step in gaining an understanding of the microstructure evolution and mechanical properties of Ti-6Al-4V cold spray coatings deposited using three feedstock powders (i.e. HDH, GA, and PA) while varying gas temperature and nozzle length.

2. Materials and methods

2.1. Cold spray processing

Three commercially available Ti-6Al-4V powders were used in this study: (1) gas atomized powder (Puris, LLC, West Virginia, USA), (2) plasma atomized powder (AP&C, Boisbriand, Quebec, Canada), and (3) hydride de-hydride powder (Phelly Materials Inc., New Jersey, USA). Cold spray deposition was performed on Ti-6Al-4V substrates (McMaster-Carr), using a VRC Gen III Max high pressure cold spray system (VRC Metal Systems, Rapid City, SD). All depositions were carried out using helium carrier gas with a gas pressure of 4.14 MPa. To evaluate the influence of particle velocity on deposition quality, gas temperature and nozzle length were varied. In this regard, three gas temperatures, i.e. 400 °C, 425 °C and 500 °C, and two nozzle lengths, i.e. 120 mm (short nozzle) and 200 mm (long nozzle), were used in this study. To prevent nozzle deterioration, high temperature depositions (i.e. 500 °C) were carried out using a two piece nozzle (tungsten-carbide converging section, polybenzimidazole (PBI) diverging section), while low temperature depositions were carried out using a PBI nozzle for both converging and diverging sections of the nozzle. All depositions were performed using a stand-off distance of 25 mm, travel speed of 200 mm/s, and deposition angle of 90°. The powder feed rate for atomized powders and hydride de-hydride powder were 5.7 g/min and 3.5 g/min, respectively. Finally, a 1-D axial model [35,36] was used to calculate particle temperature and velocity at impact, for each powder type, under the various processing conditions listed above. The particle velocity and temperature were tracked along the axis of the isentropic compressible gas flow in the nozzle [35,37]. The drag coefficient for flow around a sphere [38,39] and the forced convection heat transfer coefficient for a submerged sphere [40,41] were adopted from Bird [42].

2.2. Microstructure characterization

Optical and scanning electron microscopy (SEM) (Supra 40VP, Zeiss, Oberkochen, Germany) were used to characterize the morphology and microstructure of the as-received Ti-6Al-4V powders (i.e. HDH, PA and GA) as well as the cross-sectional microstructure of the resulting cold sprayed depositions. SEM powder morphology analysis was carried out by adhering the as-received powders on carbon tape. Powder cross-sectional analysis was performed by mounting the powder in Bakelite and subsequently subjecting the specimens to metallographic grinding/polishing using a fine SiC paper (i.e. 1200 grit) followed by coarse polishing using diamond suspensions (i.e. 9 μm, 3 μm, and 1 μm particle size) and fine polishing using alumina suspensions (1 μm, 0.3 μm, and 0.05 μm particle size). Final chemical/mechanical polishing was conducted using a mixture of colloidal silica (0.08 μm) and 30% concentrated H_2O_2. Etching was performed on the polished samples using 2% Kroll's reagent. Cold sprayed samples were sectioned along the raster (spraying) direction, mounted in Bakelite, and metallographically prepared using the procedure described above.

2.3. Nanoindentation

Nanohardness evaluation was conducted on as-received powder using a nanoindenter (MTS Nanoindenter XP, Keysight Technologies Inc., Santa Rosa, CA, USA) under load control. A maximum load of 50 mN was used and elastic modulus and hardness were recorded as a function of indention depth. For each powder type, nanohardness measurements were performed on powder particles of various sizes and the average and standard deviation were calculated. The Oliver-Pharr method [43] was used for evaluating nanohardness as well as elastic modulus. It should be noted that nanoindentation was employed (rather than microhardness) to avoid the influence of the underlying substrate (mounting compound) when testing small (~20–40 μm) powders.

2.4. Microhardness

Microhardness measurements were conducted using a Vicker's microhardness testing system (MicroMet 4, Buehler ltd., Lake Bluff, IL, USA). All measurements were performed using a load of 100 gf and dwell time of 15 s. 18–20 measurements were performed along the longitudinal direction of the coating (along the raster direction) and also through the coating thickness. Indentation diagonals were measured using an optical microscope at a magnification of 500×. To compare powder hardness to coating hardness, microhardness of powders was estimated from nanohardness data using a linear correlation [44]. The correlation takes into account the difference in area values obtained during nanoindentation and microhardness testing (projected area vs residual area of indent). To validate the accuracy of the correlation, microhardness values, estimated from the nanohardness of the PA cold sprayed coating, were compared to measured microhardness of the same coating. In this regard, nanoindentation was conducted at 20 locations throughout the thickness of the PA cold sprayed coating. The calculated and estimated microhardness values of the coating were 428 ± 19 HV0.1 and 436 ± 39 HV (estimated), respectively. It is important to note that microhardness was selected for characterizing the cold spray coatings to provide representative measurements of the cold spray coatings, while accounting for porosity.

2.5. Porosity

Porosity of the cold sprayed coatings was evaluated using ASTM standard E2109 [45]. 20 optical micrographs were collected using a magnification of 500×. To obtain representative porosity measurements, micrographs were obtained throughout the length and thickness of the coating. The latter is particularly important as coating porosity often varies as a function of thickness due to the so-called tamping effect. Porosity measurements were obtained using image analysis (Image J, NIH) and are reported as the percent porosity by area.

2.6. Adhesion strength

Adhesion strength of the cold spray coatings was measured using a tensile pull-off adhesion test according to ASTM standard D4541 [46]. Adhesion testing was performed using a portable adhesion test system (PosiTest *AT*-A, DeFelsko, Ogdensburg NY, USA). All tests were performed using a high strength adhesive (FM1000 glue, Sturbridge Metallurgical Services Inc., Sturbridge, MA) with a bond strength of 69 MPa. Specimens were tested to failure at a loading rate of 1.4 MPa/s and the maximum tensile stresses were reported as the adhesion strengths of the coating/substrate assembly. Four types of failure (depending on the weakest point in the assembly) are expected with an experiment setup in this format: (1) cohesive coating failure, (2) adhesive coating (coating/substrate interface) failure, (3) cohesive glue failure, and (4) adhesive glue (glue/coating interface) failure. The failure mode for each test was determined by visual inspection. For each treatment (powder type and process condition combination) using the short nozzle, three specimens were tested and the average and standard deviation were determined. For long nozzle, however, two specimens were tested and the average and standard deviation were reported.

3. Results and discussions

3.1. Powder characterization

The chemical compositions of the three cold spray powders (i.e. GA, PA, and HDH) are listed in Table 1. While the powders have subtle differences in primary alloy content they all exhibit a nominal composition typical of Ti-6Al-4V alloys. It is interesting to note, however, that the powders contain varying amounts of oxygen (0.20, 0.14, and 0.35 wt% for PA, GA and HDH powders, respectively), where atomized powders showed a lower oxygen content than the HDH powder. In this regard, it is well known that the hydrogenation process associated with HDH powder production commonly results in elevated oxygen content [28,47]. The influence of oxygen content on the cold spray process will be discussed in later sections.

Fig. 1 shows low and high magnification SEM micrographs of each powder type, revealing the powder morphology. From inspection of Fig. 1, powders ranged in size from < 5 μm to over 40 μm. Laser diffraction size analysis revealed the powders to have average particle sizes of 45 ± 15, 34 ± 15, and 33 ± 12 μm before sieving and 41 ± 13, 33 ± 12, and 31 ± 8 μm after sieving, for HDH, GA, and PA powder, respectively. Furthermore, from Fig. 1, the HDH powder is characterized by an irregular morphology with a rough surface texture resulting from milling, and associated particle fracture, that takes place during powder processing. The atomized powders, on the other hand, are characterized by a spherical morphology with smooth surface texture. This morphology is a result of the solidification of liquid droplets during atomization. In addition, compared to PA powders, GA powders appear to be somewhat less spherical and also contain microsatellite particles (sizes < 5 μm) attached to larger particles. The latter feature was not observed in the PA powder. PA powders are likely to be more

Table 1
Chemical compositions of as-received HDH, PA, and GA powder.

Powder type	Chemical composition (wt%)						
	Al	V	O	N	C	H	Ti
HDH	5.920	3.970	0.350	0.030	0.030	0.020	Balance
PA	6.440	4.000	0.200	0.050	0.010	0.003	Balance
GA	5.800	4.020	0.140	0.006	0.008	0.002	Balance

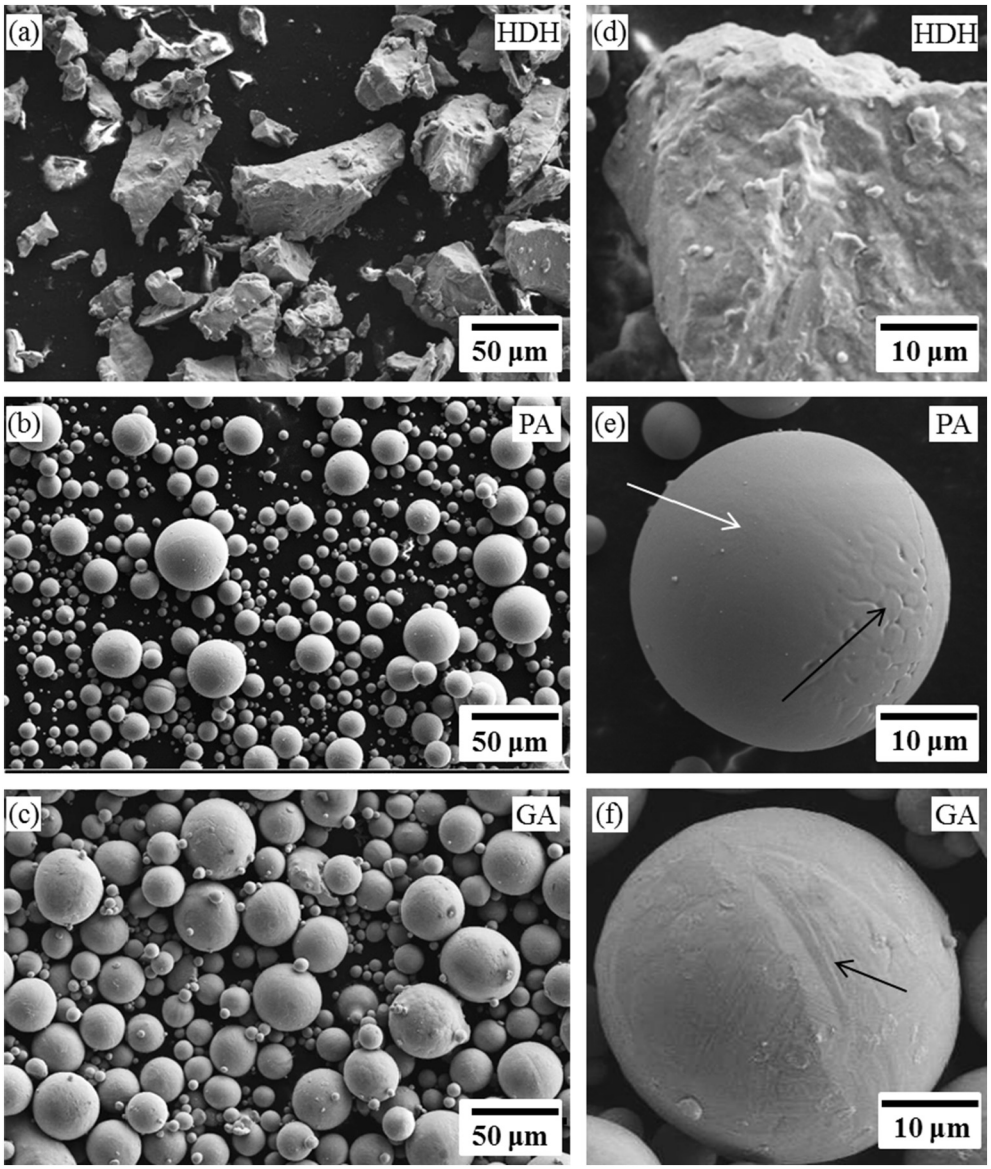

Fig. 1. Low magnification SEM images depicting the morphology of the as-received (a) HDH, (b) PA, and (c) GA Ti-6Al-4V powders. High magnification SEM images of the same powders are represented in (d) HDH, (e) PA, and (f) GA. White and black arrows in (e) represent featureless and cellular surface grain microstructures, respectively. Similarly the black arrow in (f) represents martensitic α surface grain structure.

spherical because the droplets spend more time at high temperature prior to solidification than in the case of gas atomization.

From inspection of Fig. 1(d–f), the surface structure of the powder particles may be observed. As aforementioned, HDH powders had a rough surface texture, which is a result of its processing history. The atomized powders generally had one of three surface textures: (i) equiaxed grain structures with grain sizes of 2–3 μm (Fig. 1(e), black arrow), (ii) martensitic α grain structures (Fig. 1(f), black arrow), or (iii) featureless surfaces (Fig. 1(e), white arrow). Equiaxed surface grain structures and featureless surfaces have been reported previously [26,48–50]. The featureless microstructure occurs when the powder particle undergoes rapid solidification accompanying high undercooling [51]. This can be expected in a process like atomization since the atomizing gas is introduced at a low temperature (compared to the molten metal) and at high pressure resulting in a high cooling rate. Here nucleation initiates at the surface of the atomized droplet, where undercooling is maximized. After nucleation, the solid-liquid interface advances rapidly, without solute element partitioning, resulting in a featureless surface [51,52]. As the solidification front slows, partitioning (substitutional and interstitial solute segregation) may occur and result in the formation of a cellular structure [52]. Finally, in some cases, undercooling is significantly limited and beta grains may nucleate on the particle surface and when rapidly cooled to room temperature result in the formation of martensitic α grain structures.

Fig. 2 shows SEM cross-sectional micrographs of the as-received powders in etched condition. From inspection of Fig. 2(a), the HDH powders are characterized by fine, equiaxed alpha grains with intergranular beta phase regions. Fig. 3 shows an optical metallographic image of the HDH powder that demonstrates more clearly (improved contrast) the equiaxed alpha grain structure (bright areas) with beta phase regions (dark areas) located at alpha grain boundaries. The moderate temperatures (α-β region) experienced during the hydrogenation process results in lamellar alpha phase structures with beta phase precipitated around grain boundaries. Subsequent milling of the hydrogenated powder causes a “break-up” of the lamellar alpha grains, resulting in an equiaxed alpha grain structure, as shown in Figs. 2(a) and 3. This microstructure is commonly referred to as the “mill annealed” structure and is known for its good ductility [53].

Fig. 2(b–c) shows the atomized powders are characterized by a more complicated microstructure comprising a martensitic α phase structure of various morphologies. For instance, the PA powder shown in Fig. 2(b) is characterized by needle like martensitic α phase structure, while the GA powder particle shown in Fig. 2(c) is characterized by a mixture of needle like and acicular shaped martensitic α phase. The

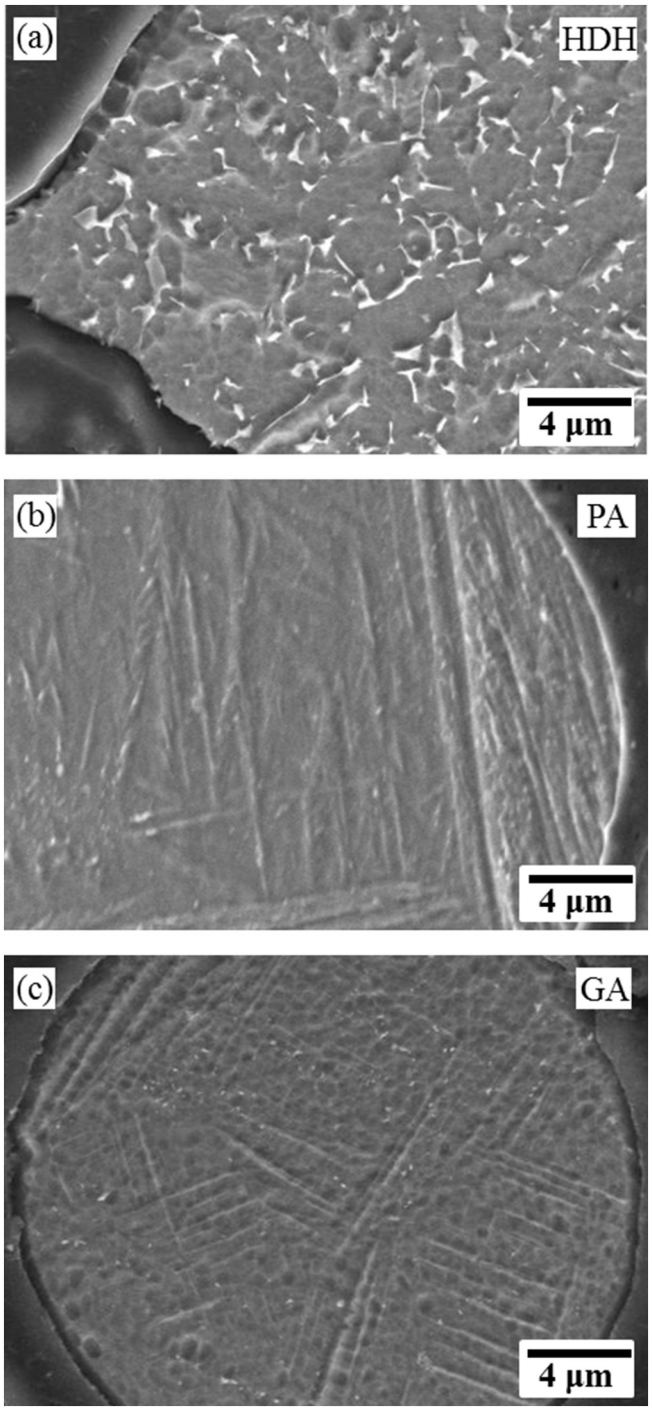

Fig. 2. SEM cross-sectional micrographs of (a) HDH (b) PA and (c) GA Ti-6Al-4V powders in as-received condition. Specimens were etched using Kroll's reagent.

shapes are somewhat difficult to distinguish, although the latter term (acicular) is typically used when the edges of alpha grains are less defined. Nevertheless, these structures both form as a result of rapid cooling from the beta phase region (≈ 980 °C) [54]. More specifically, martensitic α (α′) often forms when cooling rates exceed 410 °C/s from beyond the beta transus. Since the atomization process involves higher cooling rates (up to 10,000 °C/s) compared to the HDH process, it is expected that atomized powders are characterized by α′ grains.

It is interesting to note that the cellular and featureless structures observed on the exterior of the particles (Fig. 1(e)) are absent in the particle interiors. Once again, solidification occurs rapidly on the surface of the droplet resulting in a solid surface encapsulating partially

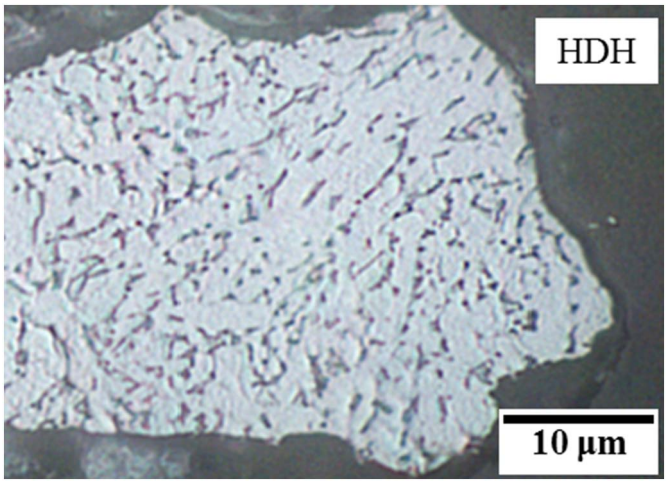

Fig. 3. Optical micrograph showing an etched cross-section of as-received HDH Ti-6Al-4V powder.

molten liquid containing a random distribution of nuclei. Since the thermal gradient is reduced inside the droplet, rapid solidification is prevented, permitting the formation of beta grains. Owing to the small size of the powder particles, the cooling rates are still high enough for a diffusionless transformation of beta grains to α′. For this reason, the particle interiors of atomized powders are characterized by α′.

Fig. 4 shows nanohardness measurements obtained from the HDH, PA, and GA feedstock powders prior to cold spray processing (gray bars). Clearly both the PA (4.35 ± 0.19 GPa) and HDH (4.32 ± 0.18 GPa) powders exhibited higher nanohardness when compared to the GA powders (3.91 ± 0.17 GPa). Although slight, the difference in nanohardness observed between these powders is most likely related to (i) powder microstructure, and (ii) oxygen content. In this regard, the atomized powders are characterized by an α′ microstructure that forms due to rapid cooling. This microstructure is expected to be much harder than the "mill annealed" structure observed in the HDH powder. The HDH powder, however, has a much higher level of oxygen content than both atomized powders. It is well established that oxygen content in Ti/Ti-6Al-4V powder can significantly impact mechanical properties [28,55]. For example, increases of up to 2.8 GPa in nanohardness have been reported for a 1 wt% increase in oxygen content in pure Ti powder [55]. Here, oxygen occupies octahedral interstitial sites in the HCP (α) titanium and strengthens the material by solid solution strengthening. Interestingly, the nanohardness of HDH powder was equivalent to PA powder despite having 75% higher oxygen content. Once again, this is attributed to the difference in

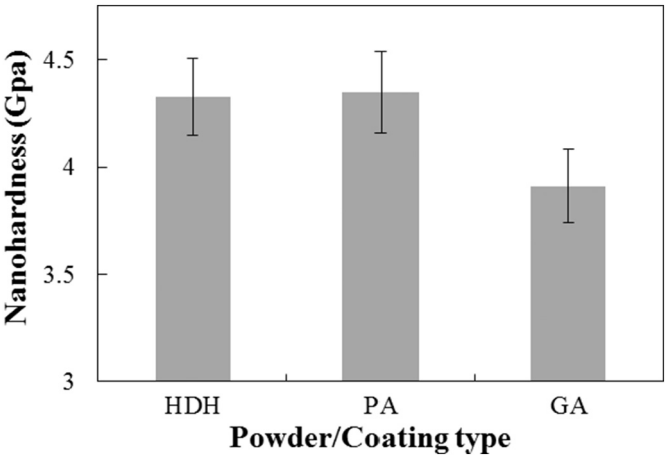

Fig. 4. Nanohardness of as-received HDH, PA, and GA Ti-6Al-4V powders.

powder microstructure. As such, low interstitial (low oxygen) HDH powder would be expected to be much softer than atomized powders. This is an important observation that may lead to the production of highly deformable HDH cold spray powders that may result in excellent deposition efficiency and improved deposition quality (e.g. low porosity). Finally, the difference in nanohardness between the GA and PA powders is attributed to the lower oxygen content observed in the GA powder.

3.2. Cold spray processing

In addition to evaluating the influence of feedstock powder type on cold spray deposition quality, this work sought to understand the influence of cold spray process parameters. As such, stagnation gas temperature as well as nozzle length, were varied for each powder type while keeping the stagnation gas pressure constant for all processing conditions. While these extrinsic processing parameters can easily be controlled during cold spray processing, the degree to which critical intrinsic variables such as impact velocity and particle temperature are affected depend on the powder size and morphology. Considering that particle impact velocity and particle temperature directly control particle deformation behavior and deposition quality, it was important to estimate these values for each powder type. Table 2 lists the estimated particle impact velocities and particle impact temperatures determined using the 1-D axial model for the three processing conditions and powder types. The model takes into account the particle size, material properties, and gas properties to estimate particle impact velocity and temperature. The difference in the velocities and temperatures observed in Table 2 were predominantly due to the difference in average powder particle size. Based on these results, it is generally expected that the deposition quality for HDH coatings would be lower than atomized cold sprayed coatings for all processing conditions, considering the lower particle velocities observed for HDH powders. It should be noted, however, that this estimation does not consider differences in powder morphology (assumes spherical particles). Powder morphology is known to influence particle acceleration in addition to other important variables (e.g., powder flowability and compressibility [56]). For the same gas temperature and pressure, compared to spherical powders, irregularly shaped powder particles may be accelerated by the carrier gas more easily due to an increase in drag force, although irregular particles also often exhibit more variability in drag coefficient [56–58]. As such, for the same particle size, irregular particles often exhibit higher particle impact velocities but significantly more variation in particle velocity [56].

In this study, process parameters were chosen to maximize particle velocities (to the extent possible in our system) while also varying particle impact temperature. Particle velocities are directly influenced by the gas velocities. Since the most important parameters affecting the gas velocities are stagnation gas pressure, temperature, and nozzle length, these parameters were chosen for our study [59,60]. Table 2 shows that an increase in gas temperature was predicted to increase the particle velocities and impact temperatures. For instance in the case of GA powder, increasing the gas temperature from 425 to 500 °C, results in an increase in particle velocity from 906 to 922 m/s and increase in impact temperature from 293 to 327 °C. Clearly, increasing the gas temperature will directly influence the temperature of the particles during flight and therefore upon impact to the substrate. Moreover, increased gas temperature also increases the thermal energy of the gas which is converted to kinetic energy at the nozzle throat resulting in increased gas velocity. It is also important to note the high stagnation pressure used for these depositions. Here, high stagnation gas pressure increases the gas density and the drag force on the powder particles. Both an increase in gas temperature and gas pressure promotes acceleration of particles in the gas stream resulting in an increase in particle velocities.

Furthermore, from inspection of Table 2, an increase in nozzle length was predicted to increase particle velocity to a larger extent than increasing gas temperature. Once again, considering the case of GA powder, increased nozzle length from 120 to 200 mm resulted in an increase in particle velocity from 906 to 933 m/s. This increase in particle velocity exists despite a slight decrease in gas temperature used with the larger nozzle (400 versus 425 °C). The rational for increased particle velocity with increased nozzle length is explained by the design of the de-Laval nozzle used in cold spray deposition. In this case, the long nozzle increases particle velocity for two reasons. First, our long nozzle design includes both an increase in nozzle length (120 to 200 mm) and an increase in expansion ratio (~200%). The latter is responsible for the gas to reach a higher Mach number. Second, the increase in the nozzle length increases the contact time between gas and particles, allowing the particles to accelerate to higher velocities. Particle impact temperatures, however, were predicted to decrease with an increase in the nozzle length. Considering the GA powder, the particle impact temperature decreased from 297 to 255 °C when transitioning from a short (120 mm) to long (200 mm) nozzle. This reduction in impact temperature occurred because of the slight decrease in gas temperature used for the long nozzle but also because the longer nozzle has a higher expansion ratio, resulting in a larger gas temperature drop along the axis of the nozzle.

3.3. Cold spray coating characterization

3.3.1. Deposition porosity

Fig. 5 shows low magnification optical micrographs of the as-deposited cold spray coatings performed using GA, PA, and HDH powders. Clearly each powder type resulted in the formation of dense cold spray coatings, although numerous triple junction and other particle-particle boundary voids are present. Qualitative comparison of the images in Fig. 5 reveals the GA powder deposition to have the lowest porosity. This is likely attributed to the reduced oxygen content, comparatively lower hardness, and higher particle impact velocity for these powders. In addition, Fig. 5 shows the coating/substrate interface is tortious. Although the cold spray process can result in particle impaction and associated substrate roughening, the nature of this interface is primarily caused by the grit blasting treatment performed on the substrate prior to deposition.

Fig. 6 shows the measured porosity for cold spray coatings

Table 2
Particle impact temperatures and velocities for each powder type and processing condition, estimated using a 1-D axial model.

Powder Type	Condition 1 Gas temperature: 425 °C Gas pressure: 4.14 MPa Nozzle length: 120 mm		Condition 2 Gas temperature: 500 °C Gas pressure: 4.14 MPa Nozzle length: 120 mm		Condition 3 Gas temperature: 400 °C Gas pressure: 4.14 MPa Nozzle length: 200 mm	
	Temperature (°C)	Velocity (m/s)	Temperature (°C)	Velocity (m/s)	Temperature (°C)	Velocity (m/s)
HDH	320	801	353	814	304	822
PA	300	882	334	897	266	908
GA	293	906	327	922	255	933

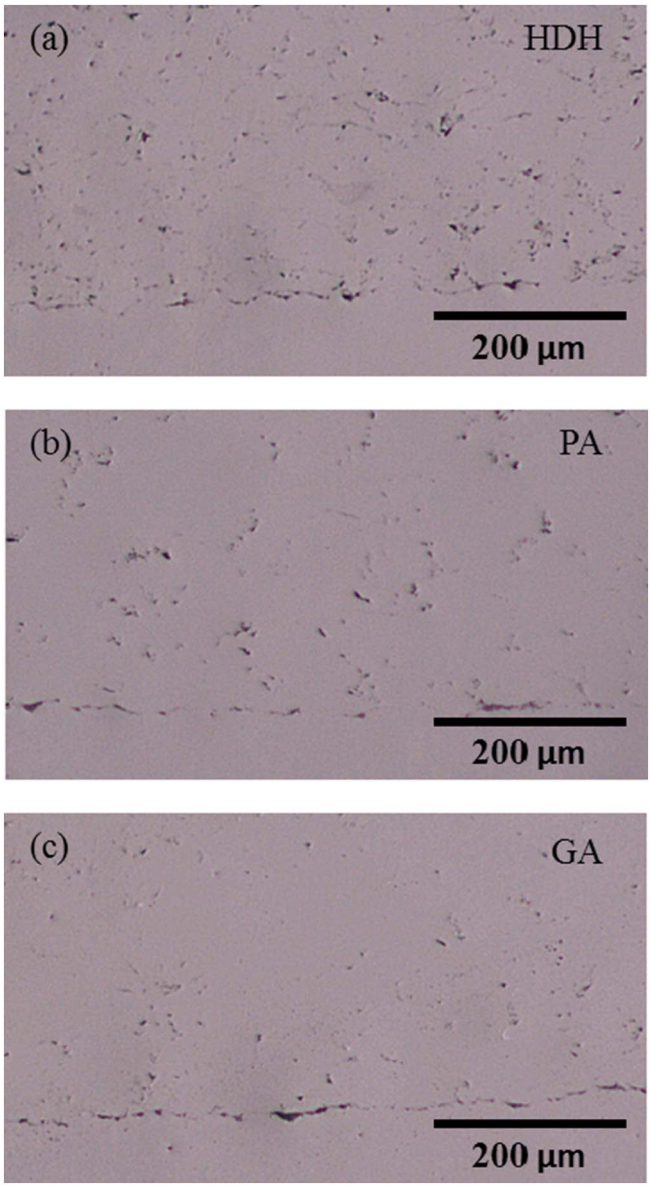

Fig. 5. Low magnification cross-sectional optical micrographs of as-deposited cold spray deposits performed at 400 °C with a long nozzle using (a) HDH, (b) PA, and (c) GA Ti-6Al-4V powders.

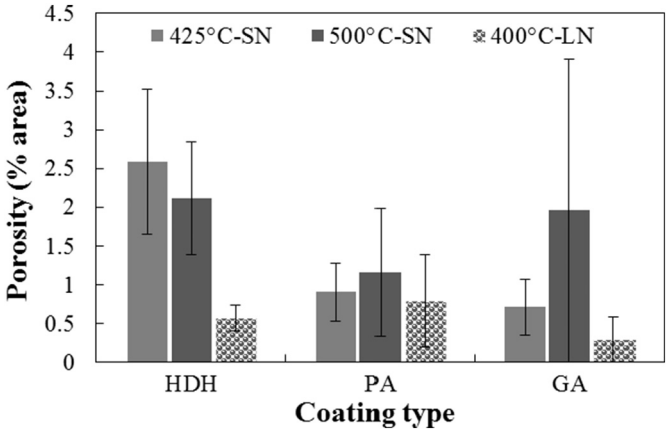

Fig. 6. Measured coating porosity as a function of gas temperature (i.e. 400, 425, and 500 °C) and nozzle length (short nozzle – SN, long nozzle – LN) for depositions produced using three types (i.e. HDH, PA, GA) of Ti-6Al-4V powder.

deposited using each powder type and with varying process conditions. From inspection of Fig. 6, each powder type produced coatings of < 1% porosity under one or more conditions. This is an important result and demonstrates the dense nature of these coatings and also the potential for further development of Ti-6Al-4V cold spray coatings. Furthermore, in all cases, coating porosity was below 3%; however, the level of porosity was significantly impacted by processing conditions. For instance, with an increase in gas temperature from 425 to 500 °C, the porosity of GA and PA cold sprayed coatings increased from roughly 1% to 2%. This increase in porosity was not expected. High particle velocities and impact temperatures (see Table 2) should generally decrease the porosity. The anomaly occurred due to nozzle fouling observed when atomized powders were deposited at higher temperatures. A similar phenomenon has been reported previously when depositing titanium alloys using helium gas at a temperature of 500 °C [4]. In this case, nozzle fouling likely occurred due to a chemical interaction between the Ti powder and tungsten carbide nozzle, resulting in the development of a thick boundary layer near the nozzle wall, leading to a reduction in gas velocity and ultimately an increase in porosity. Moreover, the large variation in coating porosity obtained for the GA powder at 500 °C is directly related to nozzle fouling. Interestingly, in contrast to the atomized powder coatings, an increase in gas temperature from 425 to 500 °C for HDH powder coatings resulted in a slight decrease in porosity (from ~2.5% to ~2%) and limited nozzle fouling. The origin of this behavior is not clear at this time; however, it may simply be due to differences in particle morphology and reduced nozzle wall contact during high temperature deposition.

Nozzle length had a dramatic impact on cold spray coating porosity for all powder types. Increasing the nozzle length from 150 to 200 mm resulted in a 78%, 12% and 59% decrease in average coating porosity for HDH, PA, and GA powders, respectively. The influence of nozzle length on cold spray coating porosity has been reported previously [60]. In this study, the reduction in porosity occurred largely as a result of the increased particle velocity achieved by using a longer nozzle. It is important to note that although particle velocities were higher, particle impact temperatures were lower when using a longer nozzle (see Table 2). Thus, particle velocity is largely responsible for the observed behavior. It should also be mentioned that the nozzle exit diameter was larger (~20%) for the long nozzle compared to the short nozzle. At the nozzle wall, gas velocity is reduced due to friction. Thus, wider nozzles permit a larger fraction of the gas and particles to flow through the nozzle with limited frictional deceleration due to nozzle wall contact [61].

Overall this work demonstrates that PA and GA powders respond to variations in cold spray processing parameters in a similar fashion, however, HDH powder responded differently. In this regard, the results indicate that the critical velocity (particle velocity beyond which high quality depositions are expected) for atomized Ti-6Al-4V powders is in the range of 900 m/s. This finding is consistent with previous reports indicating the critical velocity of Ti-6Al-4V powders to be 960 ± 200 m/s [27]. As aforementioned, when subjected to the same processing conditions (e.g. short nozzle and 425 °C gas temperature) HDH cold spray coatings contained higher levels of porosity than atomized powders. This difference in behavior is likely the result of higher oxygen content and lower particle velocities for HDH powder particles. Regarding the former, the presence of oxygen in Ti-6Al-4V powders has been reported to be detrimental to deposition quality [28]. Nevertheless, by using a long nozzle to increase the particle velocity (see Table 2) the coating porosity was reduced dramatically (Fig. 6). This suggests the critical velocity may be closer to 820 m/s for HDH powder. Nevertheless, from inspection of Fig. 6 and Table 2, there are numerous instances where the HDH particle velocity is much less than that for atomized powders while achieving similar coating porosity levels. Moreover, the critical velocity estimated here is much lower for HDH powder than for atomized powders. Critical velocity is dependent on the size of powder particles, whereby large particles are reported to

have lower critical velocities [61]. Considering the average particle size of HDH powder is 25–30% larger than that for the atomized powders used in this study, it is likely that particle size has played a significant role in lowering the critical velocity. As aforementioned (Section 3.2), it is important to note that our velocity estimations (based on a 1-D axial model) do not consider particle morphology. While it is known that increases in particle size decrease particle velocity, it is also often reported that irregular particles exhibit higher particle velocities (due to increased drag force). Considering this caveat, the HDH critical velocity estimate provided above may be a slight underestimation. In addition, although empirical relationships used to estimate critical velocity [61] often disregard powder microstructure, it is well known that the microstructure will influence deformation characteristics and therefore the required particle velocity to achieve a quality deposition. In this case, the HDH powder has an equiaxed dual-phase microstructure while the atomized powders are characterized by α′ microstructure. Thus, it is likely that the more ductile HDH microstructure may be somewhat responsible for the lower critical velocity. Finally, it should be noted that the critical velocity parameter is simply a term used to qualitatively describe the influence of particle velocity on deformation behavior and cannot be used to describe all experimental conditions or variants.

From the above discussion and from inspection of Table 2 and Fig. 6, it is clear that, for all powder types, particle velocity has a more significant influence on coating porosity than particle impact temperature. This analysis also highlights the potential for producing dense cold spray depositions using Ti-6Al-4V powders. Finally, this study also demonstrates the production of low porosity (< 2%) cold spray coatings achieved using HDH Ti-6Al-4V powders.

3.3.2. Microstructure characterization

Fig. 7 shows low and high magnification SEM micrographs of as-deposited cold spray coatings performed using HDH, PA, and GA powders, in etched condition. The low magnification images clearly show the presence of triple junction and other particle-particle interface voids (porosity) for each coating. During deposition, at the point of impact, a shock wave initiates and can result in micro-cracks near particle-particle interfaces [9]. Since Ti-6Al-4V is a hard material, micro-cracking is somewhat of a common occurrence (when compared with aluminum or copper) and difficult to eliminate completely. In addition, in some cases, grit blasting media (Al_2O_3) is present near the coating/substrate interface (Fig. 7(c)). The presence of these hard particles near the substrate interface can result in local stress concentration and premature interface failure.

Further inspection of Fig. 7(a–c) shows the Ti-6Al-4V substrate for each coating is characterized by equiaxed alpha phase with intergranular beta phase microstructure (labeled in Fig. 7(b)). Like the HDH powder, the HDH cold sprayed coatings (Fig. 7(d)) were characterized by equiaxed alpha grains with intergranular beta phase regions. The size of the beta precipitates, however, varied depending on the degree of local plastic strain experienced by the material during cold spray deposition. Regions that experienced mild to moderate deformation resulted in the particle retaining the as-received HDH powder microstructure (similar to Fig. 3) with coarse beta precipitates. This can be seen more clearly in Fig. 8(a). The retention of the as-received powder microstructure in the particle interiors is a commonly observed characteristic of cold spray depositions [9,16]. On the other hand, regions that experienced severe plastic deformation (region demarcated by double sided arrow in Fig. 7(d)) resulted in fine-scale beta precipitates and elongation of the alpha phase. Grain refinement, often located near particle-particle interfaces, is commonly observed in cold spray depositions, particularly in FCC alloys [8,9,13]. In addition to beta precipitate refinement, they are often elongated perpendicular to the deposition direction and parallel to the direction of plastic flow near the particle-particle interfaces (shown by the double-sided arrow in Fig. 7(d)). Once again, this can be observed more clearly in Fig. 8(b). This deformation behavior is attributed to high compressive stress at the point of impact [27]. The degree of plastic deformation experienced by each particle, however, was not uniform. Fig. 9 shows the microstructure of a separate individual powder particle in the cold sprayed HDH coating, where 9(a) and 9(b) correspond to low magnification SEM and optical micrographs, respectively. Fig. 9(c) provides a higher magnification SEM image obtained from the region highlighted by a dashed rectangle in Fig. 9(a) and (b). From inspection of these images, it is once again apparent that the as-received powder microstructure is retained in much of the deposited particle. Near the bottom side of the particle, however, there is a small region that exhibits, although subtly, fine, elongated beta phase and elongated alpha. Thus, this particle appears to have experienced somewhat less plastic strain compared to the particle shown in Fig. 7(d).

Like the HDH powder cold spray coatings, the atomized (GA and PA) powder coatings were characterized by two distinct microstructural regions associated with the degree of local plastic strain experienced during impact. Fig. 7(b–c) and (e–f) show that particle regions which experienced limited plastic strain are characterized by α'grains. Similar to HDH coatings, these regions were generally located away from particle-particle boundaries, particularly away from the primary impact boundary (bottom boundary). Clearly, the as-received powder microstructure is largely retained in this region, although there is some sign of martensite lath distortion that has occurred due to local plastic deformation. A second distinct microstructural region observed in atomized powders is associated with regions that experienced significant plastic strain during impact. These regions are characterized by a featureless microstructure and are often located near the primary particle impact boundary (bottom) or on the top of the particle when subjected to secondary impact from a subsequently arriving particle. For instance, Fig. 7(e–f) show a featureless microstructure band located near the particle-particle interface and demarcated with a black double-sided arrow. Clearly, the α′ structure that was present in the as-received powder is no longer present and has been supplanted by a featureless microstructure. Severe plastic deformation of the cold spray process resulted in disruption of as-received microstructure and transformation to a highly elongated structure. Considering the fact that microstructural features are not resolved at the magnification in Fig. 7(e–f), it is likely that a sub-micron or nanograin structure is present in this region. It is possible that this structure may have development due to continuous dynamic recrystallization (CDRX). However, a more thorough microstructural investigation via electron backscatter diffraction and transmission electron microscopy would be needed to confirm the mechanism. In this regard, CDRX driven nanograin formation has been suggested previously by various investigators [9,27,62] for cold sprayed Ti and Ti alloy coatings and other severe plastic deformation processes (e.g. multi-directional forging [63]). Finally, it should be noted that Birt et al. [27] reported the presence of two distinct microstructural regions when studying the microstructure of cold sprayed plasma atomized Ti-6Al-4V powder. While their results are similar in most respects, they also observed the presence of “broken” martensite laths and small clusters of β phase distributed throughout regions that experienced limited plastic strain. These features were not observed in this study, however, the reason for this discrepancy is not clear at this time. Notwithstanding, β phase decomposition along martensite laths generally occurs above 400 °C in Ti-6Al-4V [64]. Thus, the difference in behavior with respect to β phase clustering may simply be due to differences in the carrier gas temperature between these studies (i.e. 790 °C versus 400–500 °C used in this study).

3.3.3. Microhardness of cold sprayed coatings

Fig. 10 shows the microhardness of powders and cold sprayed coatings for the three powder types as a function of gas temperature and nozzle length. These measurements were performed throughout the coating thickness. The variation in hardness for each coating type is attributed to both a variation in hardness as a function of thickness and

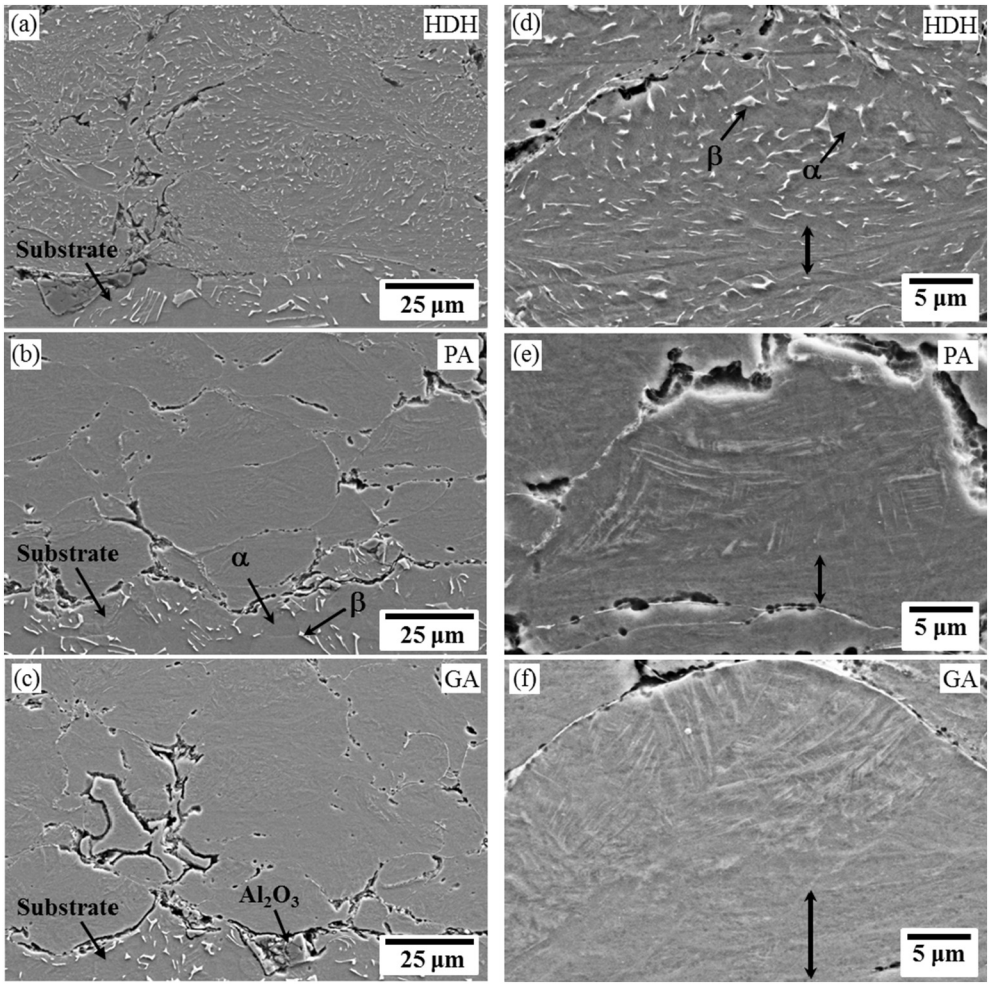

Fig. 7. Low magnification SEM images of cold spray coatings deposited at 400 °C with a long nozzle using (a) HDH, (b) PA, and (c) GA Ti-6Al-4V powder. High magnification SEM images of the same coatings are shown in (d) HDH, (e) PA and, (f) GA. The double-sided arrows in (d–f) represent severely deformed regions of individual powder particles.

to the proximity of coating porosity relative to each individual measurement. Nevertheless, general trends in microhardness as a function of processing conditions are evident. For ease in comparisons, powder microhardness values were estimated from the nanohardness measurements reported in Fig. 4. For a complete description of the estimation process and associated validation data see Section 2.4. Thus, the microhardness of the as-received HDH, PA and GA powders was 390 ± 16 HV0.1, 392 ± 17 HV0.1, and 353 ± 16 HV0.1, respectively. When using a gas temperature of 425 °C, cold spray depositions using these powders resulted in coating microhardness values of 364 ± 30 HV0.1, 414 ± 40 HV0.1, and 383 ± 42 HV0.1, respectively. Clearly, the microhardness for PA and GA coatings is somewhat higher than the respective as-received powder. Strain hardening and associated introduction of compressive residual stresses during deposition are known to increase the bulk hardness of cold sprayed coatings [65], particularly for dense deposits. In this case, PA and GA coatings have porosities below 1%, thus it is expected that the hardness would increase following cold spray deposition. For HDH coatings, on the other hand, the microhardness of the coatings (Condition 1) was lower than the as-received powder, likely a result of the comparatively higher porosity (i.e., ≈ 2.5%) of these coatings.

Fig. 10 also shows that cold spray processing parameters influenced coating microhardness, however, this influence was dependent on powder type. With an increase in gas temperature and nozzle length the microhardness of atomized cold sprayed coatings decreased and increased, respectively. The microhardness of HDH coatings, however,

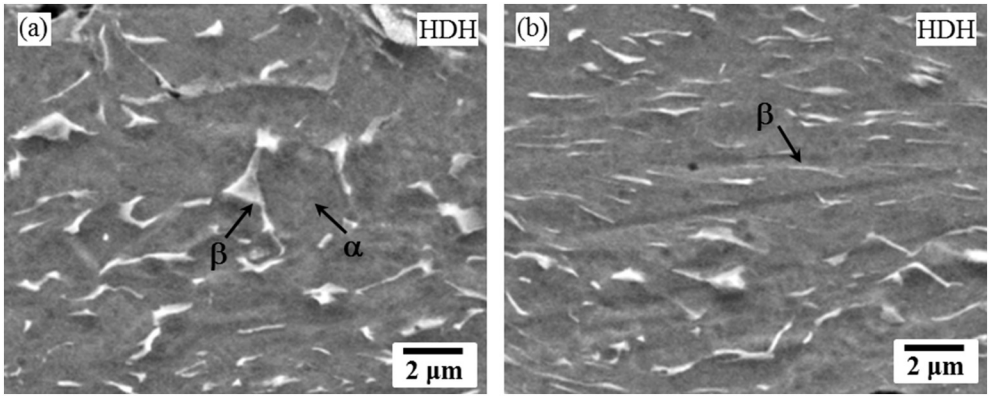

Fig. 8. (a). Higher magnification SEM images of the cold spray particle represented in Fig. 7(d), obtained from (a) a region which experienced limited plastic strain (away from the impacting interface), and (b) a region near the impact interface that experienced significant plastic strain.

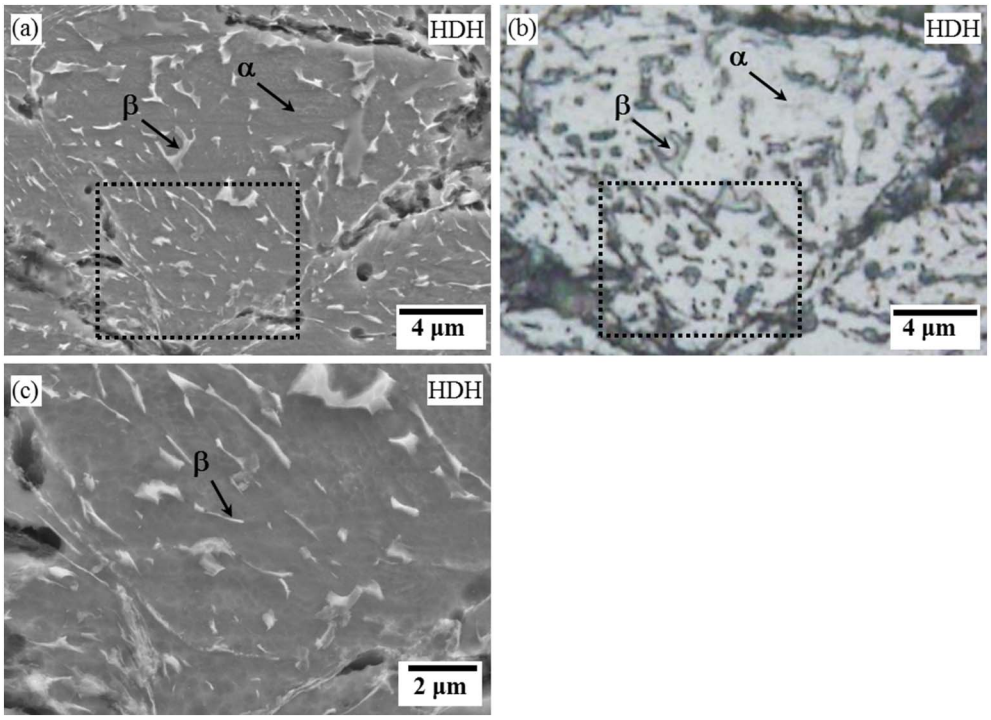

Fig. 9. Micrographs obtained from a single particle in an HDH Ti-6Al-4V cold spray coating deposited at 400 °C with a long nozzle, including (a) low magnification SEM image, (b) low magnification optical micrograph, and (c) high magnification SEM image from the region demarcated by the dashed rectangle in (a) and (b).

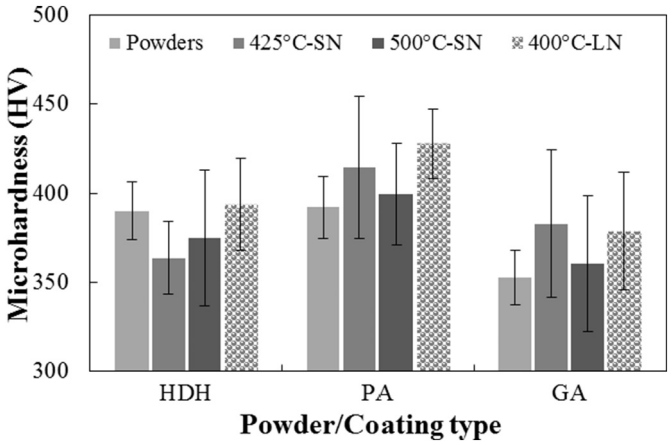

Fig. 10. Coating microhardness as a function of gas temperature (i.e. 400, 425, and 500 °C) and nozzle length (short nozzle – SN, long nozzle – LN) for depositions produced using three types (i.e. HDH, PA, GA) of Ti-6Al-4V powder. The microhardness of the as-received powders are also provided for reference and have been estimated from nano-hardness measurements provided in Fig. 4 (see Section 2.4 for details).

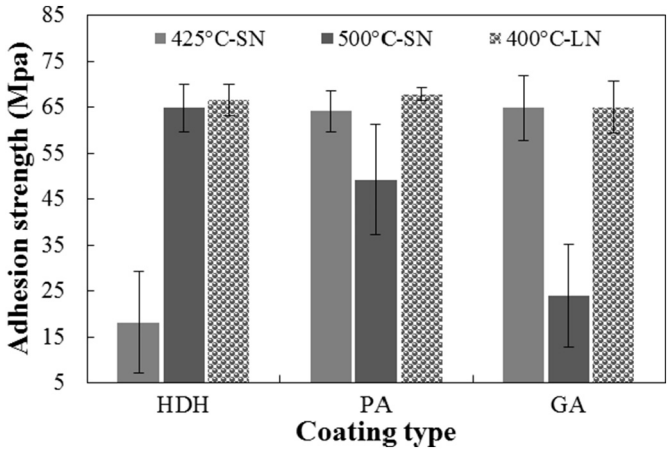

Fig. 11. Adhesion strength as a function of gas temperature (i.e. 400, 425, and 500 °C) and nozzle length (short nozzle – SN, long nozzle – LN) for depositions produced using three types (i.e. HDH, PA, GA) of Ti-6Al-4V powder.

increased for both conditions (i.e. increased gas temperature and nozzle length). In general, microhardness values corresponded well with coating porosity, i.e. decreases in coating porosity resulted in increased microhardness. In contrast to atomized coatings, however, the HDH cold spray depositions exhibited equivalent of slightly lower hardness than the as-received HDH powder, even at low porosity levels (i.e. ~0.6% when using a long nozzle). Cold spray processing typically results in strain hardening due to an increase in dislocation density [57]. In this case, however, it is possible that strain hardening was limited due to a combination of thermal softening (from adiabatic shear), slightly higher (compared to atomized powders) particle impact temperature, and lower impact velocity. The influence of thermal softening will be discussed in greater detail in the subsequent section.

3.3.4. Adhesion strength of cold sprayed coatings

Tensile pull-off adhesion testing was conducted to investigate the

Table 3
Adhesion testing failure modes observed for Ti-6Al-4V cold spray coatings deposited using three different powders and various processing conditions.

Powder type	CSP conditions	Failure mode			
		CCF[a]	ACF	CGF	AGF
HDH	425 °C - short nozzle	0	3	0	0
	500 °C - short nozzle	0	3	0	0
	400 °C - long nozzle	0	0	2	0
PA	425 °C - short nozzle	0	0	3	0
	500 °C - short nozzle	0	3	0	0
	400 °C - long nozzle	0	0	2	0
GA	425 °C - short nozzle	0	0	3	0
	500 °C - short nozzle	0	3	0	0
	400 °C - long nozzle	0	0	2	0

[a] CCF-Cohesive Coating Failure, ACF-Adhesive Coating Failure, CGF-Cohesive Glue Failure, AGF-Adhesive Glue Failure.

influence of powder type and cold spray processing conditions on the resulting coating adhesion strength. Fig. 11 provides the measured adhesion strength of cold sprayed coatings, for the three powder types, as a function of gas temperature and nozzle length. In addition, Table 3 provides a summary of the failure modes experienced for each specimen type. For high quality coatings, tensile pull-off adhesion testing is often limited by the adhesive (glue to coating adhesion) and cohesive strength (69 MPa in this case) of the glue. Thus, for samples that experienced adhesive or cohesive glue failure the 'true' adhesive strength of the coatings was not obtained, however, this does provide the minimum adhesive strength exhibited by the coating and is an indication of a sound coating.

From inspection of Fig. 11, the PA powder exhibited an adhesion strength of 64.0 ± 4.5 MPa when deposited using a gas temperature of 425 °C. With an increase in nozzle length the adhesion strength increased (67.9 ± 1.5 MPa) slightly. True comparison between the adhesion strength for these conditions cannot be made, however, considering that all samples failed by cohesive glue failure (Table 3). Nevertheless, it is generally expected that increasing particle velocity (i.e. using a long nozzle) can improve the adhesion of individual particles during the cold spray process [18] by increasing the adhesion energy [58]. With an increase in the gas temperature, however, the adhesion strength decreased (49.3 ± 11.9 MPa) and the specimens failed by adhesive coating failure. Thus, the irregular deposition quality and slight increase in porosity (i.e., 1.16 ± 0.82%) that occurred from nozzle fouling at higher temperatures also resulted in a reduction of adhesion strength. In this regard, increased coating porosity, particularly near the coating-substrate interface, can result in rapid crack propagation and premature interface failure when cracks are subjected to tensile loading such as that applied during tensile pull-off testing.

From inspection of Fig. 11, the GA coatings show similar variation in adhesion strength with changing processing parameters when compared to PA coatings. In this case, GA coatings exhibited a more pronounced reduction of adhesion strength (24.0 ± 11.1 MPa) when gas temperature was raised to 500 °C. This result in consistent with the elevated porosity observed under this processing condition and is once again attributed to nozzle fouling. Clearly, these results demonstrate that the adhesion strengths for atomized cold sprayed coatings tend to align well with coating porosity (Fig. 6), whereby high porosity results in low adhesion strength and vice versa.

Similar to atomized coatings, the adhesion strength of HDH coatings was strongly influenced by cold spray processing conditions, however, the overall behavior was markedly different. From inspection of Fig. 11, HDH coatings deposited using a gas temperature of 425 °C exhibited an average adhesion strength of 18.2 ± 11.0 MPa while failing by adhesive coating failure. With an increase in gas temperature (500 °C), the adhesion strength increased (64.8 ± 5.2 MPa) while coatings still failed by adhesive coating failure. When using a long nozzle configuration, however, the adhesion strength increased slightly (66.5 ± 3.4 MPa) but the failure mode transitioned to cohesive glue failure. Comparing these results to the measured porosity for these conditions (Fig. 6) it is once again evident that adhesion strength improved with decreasing coating porosity. In contrast to the atomized coatings, however, the adhesion strength of HDH coatings appears to be much less sensitive to elevated coating porosity. For instance, HDH coatings deposited with a gas temperature of 500 °C resulted in coating porosity of ~2%, however, these coatings had comparable adhesion strength to atomized coatings at much lower porosity levels and much greater adhesion strength when compared to atomized coatings with > 1% porosity. During the cold spray process, bonding between particles and the substrate takes place due to a combination of metallurgical bonding and mechanical interlocking. Both processes are dependent on plastic deformation whereby the former relies, in part, on the thermal energy produced during severe plastic deformation to encourage bonding. In this regard, adiabatic shear instability is well known to occur in cold spray deposition and is important for high quality depositions [18]. Adiabatic shear instability occurs near the particle interface and takes place when thermal softening in place of strain hardening. This can result in strain localization after a critical strain rate. Previously investigators have shown that alloy's initial microstructure has a strong influence on the susceptibility of the material to undergo strain localization [66–70]. Furthermore, dual phase microstructures or the presence of precipitates can promote strain localization at high strain rates [68,70]. This increase in strain localization results in a reduction in the critical velocity necessary for high quality depositions [18]. Thus, in this study, it is likely that the dual phase HDH microstructure (in combination with higher particle impact temperatures when using gas temperature of 500 °C) leaves the particles more susceptible to adiabatic shear instability and may result in stronger particle-particle and particle-substrate bonding even at elevated porosity levels. This re-emphasizes the importance of including feedstock microstructure in estimations of critical velocity. It should be noted that increased particle impact temperature alone has been reported to improve cold spray coating adhesion and cohesion strength [10,18,20]. Finally, for the reasons outlined above, the adhesion strength of HDH coatings deposited using a long nozzle, was comparable to atomized coatings (≈ 66 MPa), despite the lower estimated particle velocities of HDH powders.

Overall these results demonstrate the influence of both feedstock powder and processing conditions on Ti-6Al-4V cold spray coating adhesion strength while also demonstrating the potential for producing high quality Ti-6Al-4V cold spray coatings.

4. Conclusions

Three types of Ti-6Al-4V feedstock powders (i.e., HDH, GA, and PA) were deposited on Ti-6Al-4V substrates using a high pressure cold spray system while varying gas temperature and nozzle length. Atomized and HDH powders were characterized by a spherical and irregular external morphology, respectively. Atomized powders were characterized by α′ grain structures, whereas HDH powders comprised equiaxed α grains with β phase regions located at grain boundaries. The microstructure of the cold sprayed coatings depended on the extent of local plastic deformation experienced by the powder particles and resulted in two distinct regions. Regions that experienced low/moderate plastic strain retained the as-received powder microstructure while regions experiencing significant plastic strain were characterized either by a featureless microstructure (atomized coatings) or presence of fine, elongated beta precipitates (HDH coatings). Particle velocity had a more pronounced effect on the deposition quality when compared to particle impact temperature. In this regard, increasing the nozzle length resulted in increased particle velocities for each powder type and produced coatings with low porosity (i.e., 0.3–0.6%) and high adhesion strength (i.e., 66–69 MPa). Depositions performed using HDH powders showed comparable adhesion strength to atomized powders, albeit with higher porosity, indicating the important influence of powder microstructure on deposition quality.

Conflict of interest

The authors have no conflict of interest to disclose.

Acknowledgements

The authors are grateful for the financial support from the U.S. Army Research, Development and Engineering Command under contract no. W15QKN-16-C-0094. The authors also wish to thank James Winkels for coordinating the deposition of the material for this analysis.

References

[1] Titanium-driving growth through innovation world demand trends in airframes,

Titanium Europe, 2017 (2017 May 17–19; Amsterdam, Netherlands).
[2] B. Dutta, F.S. Froes, The additive manufacturing (AM) of titanium alloys, Met. Powder Rep. 72 (2017) 96–106 (DOI).
[4] R.E. Blose, B.H. Walker, R.M. Walker, S.H. Froes, New opportunities to use cold spray process for applying additive features to titanium alloys, Met. Powder Rep. 61 (2006) 30–37.
[5] Aviation Week Network, Supply chain research insights: global aerospace industry size and growth, http://aviationweek.com/master-supply-chain/supply-chain-research-insights-global-aerospace-industry-size-and-growth (accessed 2017 June 30).
[6] R. Jones, N. Matthews, C. Rodopoulos, K. Cairns, S. Pitt, On the use of supersonic particle deposition to restore the structural integrity of damaged aircraft structures, Int. J. Fatigue 33 (2011) 1257–1267.
[7] V. Champagne, D. Helfritch, Critical assessment 11: structural repairs by cold spray, Mater. Sci. Technol. 31 (2015) 627–634.
[8] M.R. Rokni, C.A. Widener, G.A. Crawford, Microstructural evolution of 7075 Al gas atomized powder and high-pressure cold sprayed deposition, Surf. Coat. Technol. 251 (2014) 254–263.
[9] C. Lee, J. Kim, Microstructure of kinetic spray coatings: a review, J. Therm. Spray Technol. 24 (2015) 592–610.
[10] R.R. Chromik, D. Goldbaum, M.J. Shockley, S. Yue, E. Irissou, J.-G. Legoux, N.X. Randall, Modified ball bond shear test for determination of adhesion strength of cold spray splats, Surf. Coat. Technol. 205 (2010) 1409–1414.
[11] W.-Y. Li, C. Zhang, X. Guo, J. Xu, C.-J. Li, H. Liao, C. Coddet, K.A. Khor, Ti and Ti-6Al-4V coatings by cold spraying and microstructure modification by heat treatment, Adv. Eng. Mater. 9 (2007) 418–423.
[12] M. Rokni, C. Widener, S. Ahrenkiel, B. Jasthi, V. Champagne, Annealing behaviour of 6061 aluminium deposited by high pressure cold spray, Surf. Eng. 30 (2014) 361–368.
[13] M. Rokni, C. Widener, G. Crawford, M. West, An investigation into microstructure and mechanical properties of cold sprayed 7075 Al deposition, Mater. Sci. Eng. A 625 (2015) 19–27.
[14] C. Borchers, F. Gartner, T. Stoltenhoff, H. Kreye, Microstructural bonding features of cold sprayed face centered cubic metals, J. Appl. Phys. 96 (2004) 4288–4292.
[15] M. Fukumoto, M. Mashiko, M. Yamada, E. Yamaguchi, Deposition behavior of copper fine particles onto flat substrate surface in cold spraying, J. Therm. Spray Technol. 19 (2010) 89–94.
[16] X.-T. Luo, C.-X. Li, F.-L. Shang, G.-J. Yang, Y.-Y. Wang, C.-J. Li, High velocity impact induced microstructure evolution during deposition of cold spray coatings: a review, Surf. Coat. Technol. 254 (2014) 11–20.
[17] D. Goldbaum, R.R. Chromik, Y. Stephen, E. Irissou, J.-G. Legoux, Mechanical property mapping of cold sprayed Ti splats and coatings, J. Therm. Spray Technol. 20 (2011) 486–496.
[18] D. Goldbaum, J.M. Shockley, R.R. Chromik, A. Rezaeian, Y. Stephen, J.-G. Legoux, E. Irissou, The effect of deposition conditions on adhesion strength of Ti and Ti6Al4V cold spray splats, J. Therm. Spray Technol. 21 (2012) 288–303.
[19] M.V. Vidaller, A. List, F. Gaertner, T. Klassen, S. Dosta, J.M. Guilemany, Single impact bonding of cold sprayed Ti-6Al-4V powders on different substrates, J. Therm. Spray Technol. 24 (2015) 644–658.
[20] K. Binder, J. Gottschalk, M. Kollenda, F. Gärtner, T. Klassen, Influence of impact angle and gas temperature on mechanical properties of titanium cold spray deposits, J. Therm. Spray Technol. 20 (2011) 234–242.
[21] S.H. Zahiri, W. Yang, M. Jahedi, Characterization of cold spray titanium supersonic jet, J. Therm. Spray Technol. 18 (2009) 110–117.
[22] E. Sansoucy, G. Kim, A. Moran, B. Jodoin, Mechanical characteristics of Al-Co-Ce coatings produced by the cold spray process, J. Therm. Spray Technol. 16 (2007) 651–660.
[23] P. Vo, E. Irissou, J.-G. Legoux, S. Yue, Mechanical and microstructural characterization of cold-sprayed Ti-6Al-4V after heat treatment, J. Therm. Spray Technol. 22 (2013) 954–964.
[24] S.H. Zahiri, C.I. Antonio, M. Jahedi, Elimination of porosity in directly fabricated Titanium via cold gas dynamic spraying, J. Mater. Process. Technol. 209 (2009) 922–929.
[25] C.W. Ziemian, M.M. Sharma, B.D. Bouffard, T. Nissley, T.J. Eden, Effect of substrate surface roughening and cold spray coating on the fatigue life of AA2024 specimens, Mater. Des. 54 (2014) 212–221.
[26] A.M. Birt, V.K. Champagne Jr., R.D. Sisson Jr., D. Apelian, Microstructural analysis of Ti-6Al-4V powder for cold gas dynamic spray applications, Adv. Powder Technol. 26 (2015) 1335–1347.
[27] A.M. Birt, V.K. Champagne Jr., R.D. Sisson Jr., D. Apelian, Microstructural analysis of cold sprayed Ti-6Al-4V at the micro- and nano-scale, J. Therm. Spray Technol. 24 (2015) 1277–1288.
[28] Y. Kim, E.-P. Kim, Y.-B. Song, S.H. Lee, Y.-S. Kwon, Microstructure and mechanical properties of hot isostatically pressed Ti-6Al-4V alloy, J. Alloys Compd. 603 (2014) 207–212.
[29] B. Vrancken, L. Thijs, J.-P. Kruth, J. Van Humbeeck, Heat treatment of Ti6Al4V produced by selective laser melting: microstructure and mechanical properties, J. Alloys Compd. 541 (2012) 177–185.
[30] M.H. Saleh, F. Ismail, N. Muhamad, Gas atomization of fine aluminum powder for metal injection moulding, Proceedings of 3rd international Powder Metallurgy Conference, 2002, pp. 326–336.
[31] M. Smagorinski, P. Tsantrizos, Production of spherical titanium powder by plasma atomization, Adv. Powder Metall. Part. Mater. (2002) 3–248 (DOI).
[32] C.G. McCracken, D.P. Barbis, R.C. Deeter, Key characteristics of hydride-dehydride titanium powder, Powder Metall. 54 (2011) 180–U309.
[33] J.R. Davis, Handbook of Thermal Spray Technology, ASM International, 2004.
[34] A.J. Heidloff, J.R. Rieken, I.E. Anderson, D. Byrd, J. Sears, M. Glynn, R.M. Ward, Advanced gas atomization processing for Ti and Ti alloy powder manufacturing, JOM 62 (2010) 35–41.
[35] O.C. Ozdemir, C.A. Widener, D. Helfritch, F. Delfanian, Estimating the effect of helium and nitrogen mixing on deposition efficiency in cold spray, J. Therm. Spray Technol. 25 (2016) 660–671.
[36] D. Helfritch, V. Champagne, A model study of powder particle size effects in cold spray deposition, in: U.S.A.R. Laboratory (Ed.), Aberdeen Proving Ground, MD, 2008.
[37] J.D. Anderson, Modern Compressible Flow With Historical Perspective, McGraw-Hill, Inc., New York, 2012.
[38] F.F. Abraham, Functional dependence of drag coefficient of a sphere on Reynolds number, Phys. Fluids 13 (1970).
[39] M. Van Dyke, Comments on "functional dependence of drag coefficient of a sphere on Reynolds number", Phys. Fluids 14 (1971) 1038–1039.
[40] W.E. Ranz, W.R.J. Marshall, Evaporation from drops, Chem. Eng. Prog. 48 (1952) 141–146.
[41] W.E. Ranz, W.R.J. Marshall, Evaporation from drops: part 2, Chem. Eng. Prog. 48 (1952) 173–180.
[42] R.B. Bird, W.E. Stewart, E.N. Lightfoot, Transport Phenomena, 2 ed., John Wiley and Sons, Inc, New York, 2002.
[43] W.C. Oliver, G.M. Pharr, An improved technique for determining hardness and elastic modulus using load and displacement sensing indentation experiments, J. Mater. Res. 7 (1992) 1564–1583.
[44] Correlation between nanoindentation test results and Vickers hardness, IMEKO TC3, TC5 and TC22 Conf., Metrology in Modern Context, 2010 (Pattaya, Chonburi, Thailand).
[45] ASTM E2109-01, Standard Test Methods for Determining Area Percentage Porosity in Thermal Sprayed Coatings ASTM International, West Conshohocken, PA, 2014 (2014), http://dx.doi.org/10.1520/E2109-01R14.
[46] ASTM D4541-09e1, Standard Test Method for Pull-Off Strength of Coatings Using Portable Adhesion Testers ASTM International, West Conshohocken, PA (2009), (2009), http://dx.doi.org/10.1520/D4541-09E01).
[47] C.R.F. Azevedo, D. Rodrigues, F.B. Neto, Ti-Al-V powder metallurgy (PM) via the hydrogenation-dehydrogenation (HDH) process, J. Alloys Compd. 353 (2003) 217–227.
[48] G.J. Marshall, E.K. Loannidis, T. Sheppard, Microstructural characterization of rapidly solidified Al-Mg-Mn powder alloy, Metall. Trans. A. 18 (1987) 407–416.
[49] A. Srivastava, S. Ojha, S. Ranganathan, Microstructural features and heat flow analysis of atomized and spray-formed Al-Fe-V-Si alloy, Metall. Mater. Trans. A 29 (1998) 2205–2219.
[50] J.R. Groza, J.F. Shackelford, Materials Processing Handbook, CRC press, 2007.
[51] H. Jones, Microstructure of rapidly solidified materials, Mater. Sci. Eng. 65 (1984) 145–156.
[52] E. Lavernia, The evolution of microstructure during spray atomization and deposition, Int. J. Rapid Solidification 5 (1989) 47–85.
[53] H. Chandler, Heat Treater's Guide: Practices and Procedures for Nonferrous Alloys, ASM International, 1996.
[54] T. Ahmed, H.J. Rack, Phase transformations during cooling in alpha + beta titanium alloys, Mater. Sci. Eng. A Struct. Mater. Prop. Microstruct. Process. 243 (1998) 206–211.
[55] B. Sun, S. Li, H. Imai, J. Umeda, K. Kondoh, Oxygen solid solution strengthened pure titanium powder materials, Trans. JWRI 41 (2012) 59–64.
[56] W. Wong, P. Vo, E. Irissou, A. Ryabinin, J.-G. Legoux, S. Yue, Effect of particle morphology and size distribution on cold-sprayed pure titanium coatings, J. Therm. Spray Technol. 22 (2013) 1140–1153.
[57] N. Cinca, J.M. Rebled, S. Estrade, F. Peiro, J. Fernandez, J.M. Guilemany, Influence of the particle morphology on the Cold Gas Spray deposition behaviour of titanium on aluminum light alloys, J. Alloys Compd. 554 (2013) 89–96.
[58] T. Hussain, Cold spraying of titanium: a review of bonding mechanisms, microstructure and properties, Key Eng. Mater. Trans Tech Publ. (2013) 53–90.
[59] A.P. Alkhimov, V.F. Kosarev, S.V. Klinkov, The features of cold spray nozzle design, J. Therm. Spray Technol. 10 (2001) 375–381.
[60] K. Sakaki, Y. Shimizu, Effect of the increase in the entrance convergent section length of the gun nozzle on the high-velocity oxygen fuel and cold spray process, J. Therm. Spray Technol. 10 (2001) 487–496.
[61] C.M. Kay, J. Karthikeyan, High Pressure Cold Spray-Principles and Applications, ASM International, 2016.
[62] K. Kim, M. Watanbe, J. Kawakita, S. Kuroda, Grain refinement in a single titanium powder particle impacted at high velocity, Scr. Mater. 59 (2008) 768–771.
[63] T. Sakai, A. Belyakov, R. Kaibyshev, H. Miura, J.J. Jonas, Dynamic and post-dynamic recrystallization under hot, cold and severe plastic deformation conditions, Prog. Mater. Sci. 60 (2014) 130–207.
[64] W. Xu, M. Brandt, S. Sun, J. Elambasseril, Q. Liu, K. Latham, K. Xia, M. Qian, Additive manufacturing of strong and ductile Ti–6Al–4V by selective laser melting via in situ martensite decomposition, Acta Mater. 85 (2015) 74–84.
[65] V.K. Champagne, D.J. Helfritch, M.D. Trexler, B.M. Gabriel, The effect of cold spray impact velocity on deposit hardness, Model. Simul. Mater. Sci. Eng. 18 (2010) 065011.
[66] M. Meyers, Plasticity: adiabatic shear localization, Encyclopedia of Materials: Science and Technology, 2001, pp. 7093–7103.
[67] H. Zhan, W. Zeng, G. Wang, D. Kent, M. Dargusch, Microstructural characteristics of adiabatic shear localization in a metastable beta titanium alloy deformed at high strain rate and elevated temperatures, Mater. Charact. 102 (2015) 103–113.
[68] W.-S. Lee, T.-H. Chen, C.-F. Lin, G.-T. Lu, Adiabatic shearing localisation in high strain rate deformation of Al-Sc alloy, Mater. Trans. 51 (2010) 1216–1221.
[69] A. Odeshi, S. Al-Ameeri, M. Bassim, Effect of high strain rate on plastic deformation of a low alloy steel subjected to ballistic impact, J. Mater. Process. Technol. 162 (2005) 385–391.
[70] A. Odeshi, M. Bassim, Evolution of adiabatic shear bands in a dual-phase steel at very high strain rates, Mater. Sci. Eng. A 488 (2008) 235–240.